University of Bath

Alternative formats

If you require this document in an alternative format, please contact:
openaccess@bath.ac.uk

A comparison of the pulsed, lock-in and frequency modulated thermography nondestructive evaluation techniques[☆]

Krishnendu Chatterjee[a,*], Suneet Tuli[a], Simon G. Pickering[b], Darryl P. Almond[b]

[a]*Centre for Applied Research in Electronics, Indian Institute of Technology, Delhi 110016, India*
[b]*UK Research Centre in NDE, Department of Mechanical Engineering, University of Bath, Bath BA2 7AY, UK*

Abstract

Pulsed, lock-in and frequency modulated thermography are three alternative nondestructive evaluation techniques. The defect imaging performance of these techniques are compared using: matched excitation energy; the same carbon fiber composite test piece and infrared camera system. The lock-in technique suffer from "blind frequencies" at which phase images for some defects disappear. It is shown that this problem can be overcome by using frequency modulated (chirp) excitation and an image fusion algorithm is presented that enhance phase imaging of defects. The signal-to-noise ratios (SNR) of defect images obtained by the three techniques are presented. For the shallowest defects (depths 0.25 and 0.5 mm, 6 mm diameter), the pulsed technique exhibits the highest SNRs. For deeper defects the SNRs of the three techniques are similar in magnitude under matched excitation energy condition.

Keywords: Pulsed thermography, Lock-in thermography, Blind frequency, FMTWI, Matched energy comparison, Image fusion

1. Introduction

Pulsed [1, 2] and lock-in [3] thermography are the most commonly used thermographic nondestructive evaluation techniques. The two techniques are distinctly different but are deployed in the inspection of similar components/structures. In general these techniques are suitable for the detection of shallow planer defects, *e.g.* delamination in composites or adhesion defect in surface coatings.

In pulsed thermography, the sample surface is instantaneously heated using an optical flash. Over time the surface heat penetrates into the material producing asymptotic cooling. If sub-surface faults are present, heat-flow is obstructed. These result in relatively slower cooling of the defective regions than their sound counterparts. Consequently relative hot spots appear on the surface above the defects. The hot-spots thus obtained in pulsed thermography eventually fade away to achieve thermal equilibrium.

By contrast, in lock-in thermography the sample surface is heated by periodically modulated lamps and thermograms are captured under the periodic sinusoidal heating. The analysis of these thermograms mainly considers the phase shift of the thermal response of the defective regions with respect to the sound regions of

the material [3]. Fourier transformation is extensively used for this purpose. The phase and magnitude information, thus obtained for each of the pixels in the thermogram, are stored in the form of 2D-matrices and subsequently converted into a gray scale images known as the phase image and magnitude image. Since in this technique, the images are extracted at the same frequency as used in the excitation, it is called lock-in thermography with an analogy to the working principle of lock-in amplifier. The excitation frequency is chosen based on the diffusion length of the thermal signal. The thermal diffusion length is the distance over which the signal strength falls to $1/e$ of that at the surface. Since the material acts as a low-pass filter, lower frequency signals propagate further into the material. However if the defect lies beyond the diffusion length, it is not likely to be seen.

Since, pulsed and lock-in thermography are intrinsically different, their comparison is problematic. An objective comparison between them, based on the estimation of the signal-to-noise ratio between the defective regions and the background noise under matched excitation energy condition on a carbon fiber composite, was reported earlier [4]. It showed the superiority of the pulsed technique over lock-in for shallower defects. However, for deeper defects the performances of the techniques were similar. In the comparison, lock-in phase images were chosen over magnitude images as they are least affected by the variation of surface emissivity and illumination. However, the presence of blind frequencies [5, 6, 4] poses a major problem in the utilization of phase images in lock-in thermography. These are the frequencies at which the defect does not exhibit any phase shift with respect to the sound region although

the thermal diffusion length is longer than the depth of the defect. This effect is primarily a 3-dimensional heat-flow phenomenon which cannot be accounted for using a traditional one dimensional heat-flow model. Thus if lock-in thermography is performed at only one frequency, there is always a chance of overlooking some of the defects in the phase image. Of course the inspection can be repeated over multiple frequencies to avoid the short-coming but certainly this increases its duration. This paper proposes an application of a relatively new thermographic technique, named frequency modulated thermal wave imaging (FMTWI) [7, 8], as a means of overcoming the problem of blind frequencies. The excitation, presently used in FMTWI, comprises of a linear up-chirp whose bandwidth spans over the frequencies necessary to produce thermal diffusion lengths to cover the range of defect depths in question. As per Fourier theorem, such a signal may be viewed as a superposition of multiple sinusoidal signals having frequencies which are integral multiples of the fundamental. Thus FMTWI, in essence, can be termed as superposed lock-in thermography which facilitates extraction of multiple phase and magnitude images from a single run without lengthening its duration.

In contrast to pulsed excitation, where a large number of frequencies constructively interfere at an instance in time, in FM excitation, the constructive interference is absent due to the nature of phase distribution over the constituent frequencies. However, using signal processing, it is possible to make them interfere to generate a pulse-like response. This technique is known as pulse compression, and was mentioned as a major advantage of FMTWI over lock-in technique [7]. Matched filtering is used to achieve this. In the matched filter, individual constituent frequencies are delayed in such a way that they produce constructive interference at the output of the filter.

This paper compares the image quality obtained from FMTWI to that obtained from pulsed and lock-in techniques. Finally, as a measure to overcome the problem of blind frequencies, an image fusion algorithm is proposed and demonstrated.

2. Test piece

Figure 1 is a drawing of the test piece employed in all tests described in this paper. It is an approximately 7 mm thick carbon fiber composite board containing artificial defects formed by sets of 2, 4 and 6 mm diameter flat-bottomed holes at depths from the surface ranging from 0.25 mm to 2.5 mm in 0.25 mm increments. The four 12 mm diameter holes at the edge of the sample are at depths of 2, 2.5, 3 and 3.5 mm. The test piece was painted with acetone soluble black acrylic paint to provide a greater surface absorptivity and to reduce the effects of spurious reflections from the lamps, camera and surroundings. Only the 6 mm diameter defects are considered for this work.
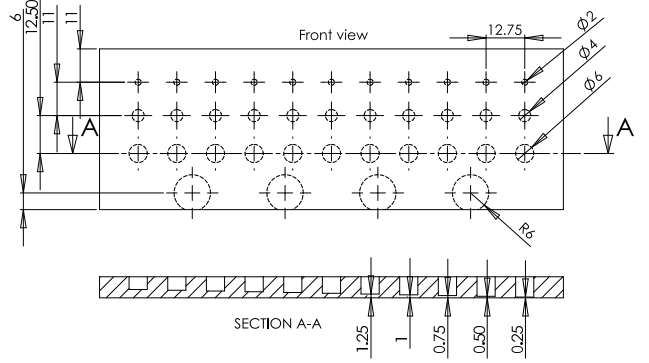

Figure 1: Test piece dimensions (all in mm.)

Table 1: Thermal diffusion length as a function of frequency for carbon fiber composite

Frequency (mHz)	Diffusion length (mm)
10	8.1
20	5.7
30	4.7
40	4.1
50	3.6
60	3.3
70	3.1
80	2.9
90	2.7

3. Choice of frequencies in lock-in and FMTWI

Both in lock-in thermography and FMTWI, the target is periodically heated using external heat sources, which produce highly attenuated thermal waves inside the material. The possibility that a defect can be detected by such a wave depends on its depth being less or similar to the thermal diffusion length. The thermal diffusion length (μ), the distance over which the wave's amplitude falls to $1/e$ of that at the surface, is a measure of its attenuation factor. μ is related to the excitation frequency and material properties (thermal conductivity K, density ρ and specific heat c) through

$$\mu = \sqrt{\frac{2k}{\omega \rho c}} \qquad (1)$$

where ω is the angular frequency.

The thermal diffusion lengths for a typical carbon fiber composite material having $K = 4$ W/m °C, $\rho = 1600$ Kg/m^3 and $c = 1200$ J/Kg °C at various excitation frequencies are listed in table 1. Practically any frequency in the range of 10 mHz to 90 mHz can be used for lock-in tests. However in view of the current comparison work with FMTWI, the choice becomes restricted. Presently in FMTWI, a linear up-chirp is used.

3

Table 2: Test durations for various excitation schemes

Scheme —	Frequency (mHz)	Test duration (seconds)
FMTWI	20 to 80	60
Lock-in	16.7	180
	33.3	90
	50.0	60
	66.7	45
	83.3	36

The phase (ϕ) of such a signal is related to time (t) as

$$\phi = 2\pi \left(f_i + \frac{kt}{2} \right) t + \phi_i \qquad (2)$$

where f_i is the initial frequency of the chirp, k is the frequency slope and ϕ_i is the initial phase, *i.e.* phase at time $t = 0$. The terminal phase and the initial phase of the chirp should differ only by integral multiples of 2π. Otherwise during the Fourier transformation of the signal, which implicitly assumes that the waveform repeats itself in time, high frequency components would be generated due to the presence of discontinuities at the repetition boundaries. Hence the initial phase ($\phi|_{t=0}$) and the final phase ($\phi|_{t=\tau}$) of the chirp should be related to each other by

$$\phi|_{t=\tau} = \phi|_{t=0} + 2n\pi \qquad (3)$$

where τ is the duration of the chirp and n is the number of oscillation the signal completes in τ. This relates the chirp bandwidth, its duration and the number of complete oscillations as

$$\tau = \frac{2n}{f_i + f_f} \qquad (4)$$

where f_f is the final frequency at $t = \tau$. Thus for the current work, a chirp with 20 mHz initial frequency and 80 mHz final frequency is chosen which nicely exhibits 3 complete oscillations in 60 seconds. In this frequency range, the thermal diffusion lengths span over 5.7 mm to 2.9 mm, table 1, which is 40% of the thickness. As the signal repeats itself in every 60 seconds, Fourier transformation of the signal produces 16.7 mHz as the fundamental frequency and 33.3 mHz, 50.0 mHz, 66.7 mHz, 83.3 mHz as harmonics. Higher harmonics beyond 83.3 mHz are not significant as they fall significantly outside the bandwidth of the chirp. Thus the processing of FMTWI data produces five meaningful magnitude and phase images which are compared with those obtain from lock-in thermography tests performed at identical frequencies. In each lock-in case, the duration of the experiment is adjusted in order to accommodate three complete oscillations of the sinusoidal excitation. Table 2 shows the test durations. It may be noted that the application of pulse compression would not produce any significant result in the present case, as the time-bandwidth product (60mHz × 60sec = 3.6) is very low.

4. Energy Matching

In order to make an objective comparison of pulsed, lock-in and FMTWI techniques, the effective excitation energies for each of the techniques have to be made identical. In pulsed thermography, the energy is fixed by the flash lamp and its driver electronics while in lock-in and FMTWI, the test piece is periodically heated using tungsten-halogen flood lamps whose power and time of exposure can be readily adjusted. Since these lamps cannot take away any energy from the test piece, their periodic heating resembles that obtained from an alternating heat source superposed on a DC background. The DC part merely increases the average temperature of the test piece and does not take part in the lock-in and FMTWI experiment. It is only the AC part which creates a thermal wave and is responsible for the phase and magnitude images. Thus in order to compare the thermographic techniques, the pulsed energy should be matched only to the alternating part of the heat energy in lock-in and FMTWI tests. It may be noted that the proposed energy matching is applicable only in time domain and not in frequency domain. Here we are making a matching of the total excitation energies employed in the various techniques. For a comparison of pulse with FMTWI, it could be argued that the pulse energy should be matched to that of the frequency component of the linear chirp used to generate the images concerned. Or alternatively, the energy of a lock-in test should be matched to the energy of the frequency components of pulse excitation involved in the generation of a pulse image of a particular defect. However, in practice it seems reasonable to obtain an indication of relative performance of the technique for a given total necessary energy of excitation. The following sections describe how time domain energy matching is achieved amongst pulsed, lock-in and linear FMTWI techniques.

4.1. Pulsed Thermography

In a pulsed thermography experiment, if E_P energy is absorbed per unit area of the test piece, its surface temperature's time evolution (T_P) is known to be

$$T_P = \frac{E_P}{2e\sqrt{\pi t}} \qquad (5)$$

where e is the effusivity of the material. Thus if T_P is measured at $t = 1$ second, E_P can be estimated from

$$E_P = T_P \Big|_{t=1} 2e\sqrt{\pi} \qquad (6)$$

4.2. Lock-in Thermography

In lock-in thermography, performed at an angular frequency ω, the excitation (W) has the generic form

$$W = W_{DC} + W_0 \sin \omega t \qquad (7)$$

where for all real heat sources $W_0 \leq W_{DC}$. However, only the sinusoidal term contributes to the surface temperature oscillation whose amplitude (T_{AC}) is mathematically related to the AC peak power per unit surface
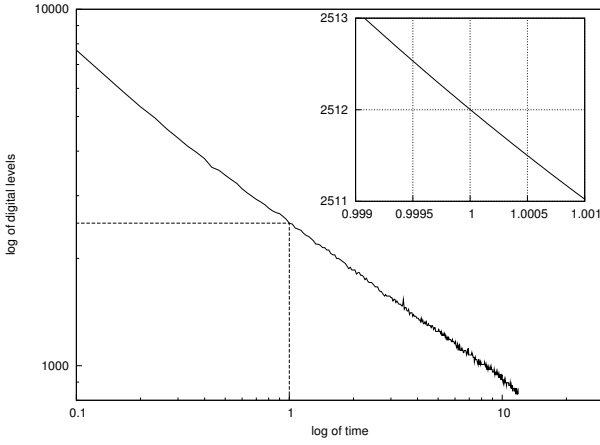
Figure 2: Plot of logarithmic temperature rise (digital level) against logarithmic time over sound region in pulsed thermography experiment. The inset plot zooms around t = 1 second.

area (W_0) by

$$T_{AC} = \frac{W_0}{e\sqrt{\omega}} \qquad (8)$$

Thus the total effective AC thermal energy exchanged through unit surface area per cycle (Q_{LI}) is

$$
\begin{aligned}
Q_{LI} &= 2\int_0^{\frac{\tau}{2}} W_0 \sin\omega t \, dt \\
&= \frac{4W_0}{\omega} \qquad (9)
\end{aligned}
$$

where (τ = Time period = $\frac{2\pi}{\omega}$). Consequently the total AC energy exchanged during the entire lock-in thermography experiment of duration D through the test piece's unit surface area = $E_{LI} = Q_{LI} \times N$ where $N = D/\tau$ = the total number of heating cycle the test piece underwent during the experiment. Thus

$$
\begin{aligned}
E_{LI} &= \frac{4W_0}{\omega} \times \frac{D}{\tau} \\
&= \frac{2W_0 D}{\pi} \qquad (10)
\end{aligned}
$$

Substituting the expression of W_0 in equation 10 from equation 8

$$E_{LI} = \frac{2D}{\pi} \times e\sqrt{\omega} \times T_{AC} \qquad (11)$$

To carry out the comparison between pulsed and lock-in thermography experiment under matched-energy condition, E_P (from equation 6) and E_{LI} (from equation 11) are equated

$$
\begin{aligned}
T_P\Big|_{t=1} 2e\sqrt{\pi} &= \frac{2D}{\pi} \times e\sqrt{\omega} \times T_{AC} \\
T_{AC} &= \frac{\pi \, T_P\big|_{t=1}}{D\sqrt{2f}} \qquad (12)
\end{aligned}
$$

An example of the experimental determination of $T_P\big|_{t=1}$ is shown in figure 2. This figure shows the temperature recorded by an infrared camera in terms of the

Table 3: Estimated amplitude of surface temperature oscillations for lock-in tests at various frequencies as imposed by the energy matching criterion

Frequency	Duration	Estimated T_{AC}
mHz	Seconds	Digital levels
16.7	180	240
33.3	90	340
50.0	60	416
66.7	45	481
83.3	36	537

digital levels for a pixel over a sound area of the test piece.

In order to equalize the total AC energy, the amplitude of surface temperature oscillation in lock-in tests (T_{AC}) from equation 12 must as per table 3.

Thus prior to the experiment, the external heat sources were approximately tuned to achieve the aforesaid surface temperature oscillation amplitudes. Figure 3a to 3e show the experimentally observed offset-subtracted surface temperature variation of the test piece under energy matched lock-in tests at various frequencies.

4.3. Linear FMTWI

In linear FMTWI, the excitation can also be broken into DC and AC components. As in the case of lock-in, only the AC component contributes to the surface temperature oscillation. The signal phase for such linear up-chirp with initial frequency f_0 and frequency slope k, varies with time as

$$\phi = 2\pi\Big(f_0 + \frac{kt}{2}\Big)t \qquad (13)$$

Consequently E_{FM}, the effective AC energy exchanged through unit surface area during the entire FMTWI test of duration D, is

$$E_{FM} = \int_0^D W_0 \left| \sin\left(2\pi\Big(f_0 + \frac{kt}{2}\Big)t\right) \right| dt \qquad (14)$$

where W_0 is the amplitude of the heating. Since this integral is not analytically solvable, integrating it numerically with $f_0 = 20$ mHz, $k = 1$ mHz/second and $D = 60$ seconds yields

$$E_{FM} = 37.9W_0 \qquad (15)$$

which is almost identical to the total AC energy transferred in a 3 cycle 50 mHz, 60 second lock-in test as calculated from equation 10.

$$E_{LI} = \frac{2 \times 60 \times W_0}{\pi} = 38.2W_0 \qquad (16)$$

Thus the same excitation amplitude can be used to perform the FMTWI under the matched energy condition as in 50.0 mHz lock-in. The experimentally observed surface temperature variation as a function of time is shown in figure 3f under this condition. It is interesting to note that the amplitude of these oscillations decreases with increase in frequency, although the amplitude of the applied heating is kept constant.
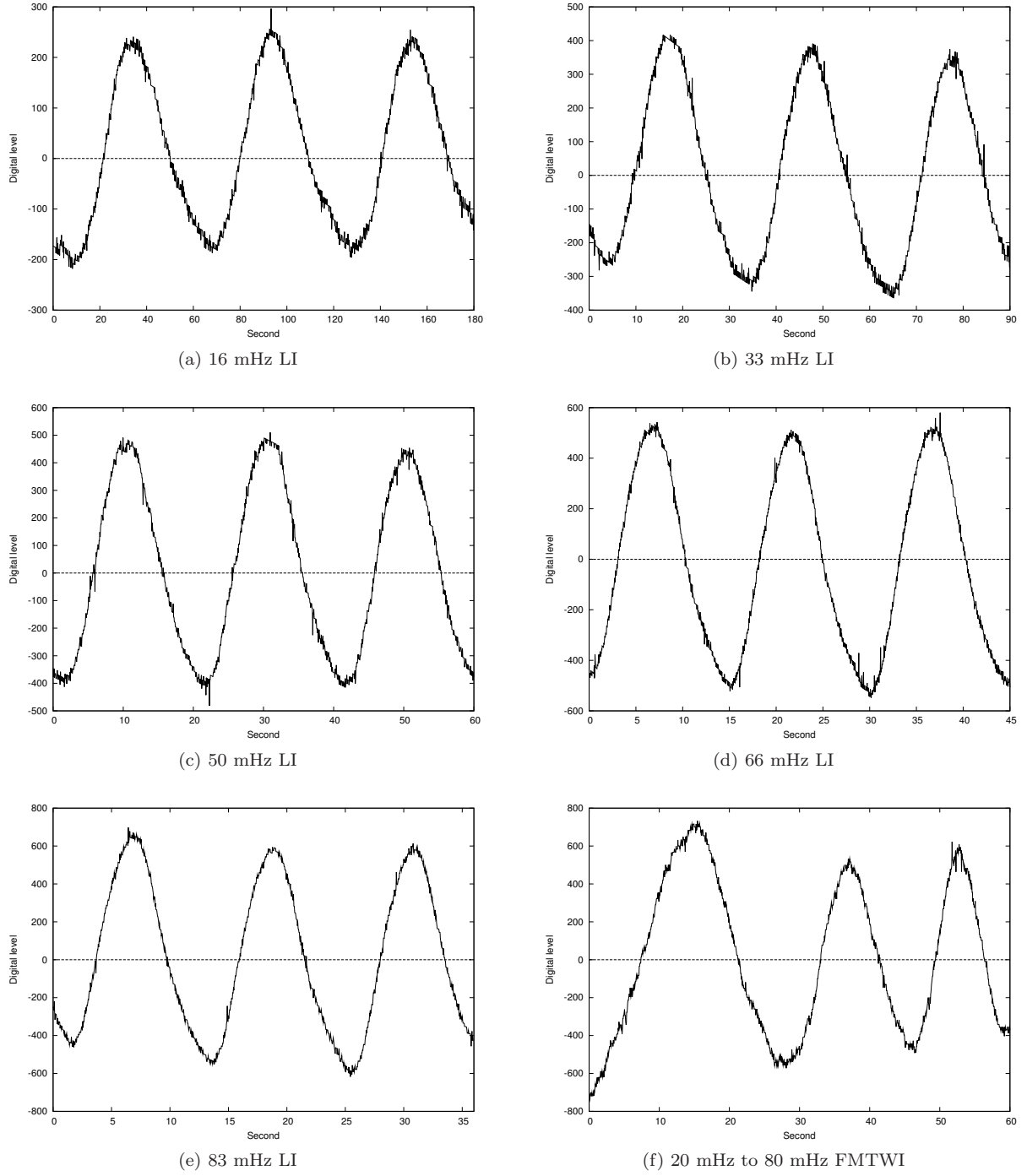
5

(a) 16 mHz LI

(b) 33 mHz LI

(c) 50 mHz LI

(d) 66 mHz LI

(e) 83 mHz LI

(f) 20 mHz to 80 mHz FMTWI

Figure 3: 3a-3e: Thermal oscillations obtained in lock-in thermography experiments on sound region at the frequencies indicated. 3f: FMTWI thermal oscillations observed on the sound region, indicating frequency increase with time.

5. Data processing

5.1. Calculation of phase and amplitude images in lock-in and FMTWI

There are two steps in the process — a) offset trend removal and b) Fourier transformation. The former is essential because of the presence of DC heating which gradually ramps up the average temperature of the test piece. The Fourier transformation is erroneous under such a condition. To remove the trend, straight lines are fitted to the time varying temperature data pixel by pixel using a least square fit algorithm and then the fitted trend is subtracted from the original data. Once the offset trend is removed, the Fourier transforms of the trend subtracted thermal signals (T_{AC}) are carried out in the following way.

$$I_{\sin} = \int_0^D T_{AC}(t) \, \sin \omega t \, dt \qquad (17)$$

$$I_{\cos} = \int_0^D T_{AC}(t) \, \cos \omega t \, dt \qquad (18)$$

6

$$\phi = \tan^{-1}\left(\frac{I_{\cos}}{I_{\sin}}\right) \qquad (19)$$

$$A = \sqrt{I_{\sin}^2 + I_{\cos}^2} \qquad (20)$$

where ω is the angular frequency of interest. For lock-in tests, it is same as the excitation frequency used during the experiment. The 2-dimensional representations of A and ϕ, converted to gray-scale, constitute the magnitude and phase images respectively.

5.2. Estimation of Signal-to-Noise Ratio

In a thermogram or a phase/magnitude image, signal is defined as the difference between the response of a region over a defect to that of the same region had the defect been not there. The hypothetical sound region can be constructed over a defective region by a surface fit as described in the following sections. The noise is taken to be the standard deviation of image/pixel data from the same fitted surface, excluding the defective regions.

5.2.1. 3D Surface Fit

A thermogram or a phase/magnitude image may be visualized as a 3D surface where X- and Y-directions represent pixels and Z-direction represents either temperature, phase or magnitude. The following is the surface which is to be fitted to the image.

$$z = \sum_{i=0}^{R}\sum_{j=0}^{R} a_{ij}x^i y^j \qquad (21)$$

The error (E) of the fit is

$$E = \sum_{k=1}^{N}\left(\sum_{i=0}^{R}\sum_{j=0}^{R} a_{ij}x_k^i y_k^j - z_k\right)^2 \qquad (22)$$

where z_k is the original value at pixel (x_k, y_k) and N is the total number of pixels. To minimize the error, the partial derivatives of E with respect to each of the coefficients (a_{pq}) are equated to zero.

$$\frac{\partial E}{\partial a_{pq}} = 0 \qquad (23)$$

which leads to the following relationship.

$$\sum_{i=0}^{R}\sum_{j=0}^{R} a_{ij}\left(\sum_{k=1}^{N} x_k^{i+p} y_k^{j+q}\right) = \sum_{k=1}^{N} x_k^p y_k^q z_k \qquad (24)$$

This is a set of linear equations in a_{ij} which are solved to get their values and hence the fitted surface.

5.2.2. Avoiding Local Features

The drawback of the least square fit algorithm, described above, is that it does not discriminate between the sound and the defective regions in the thermogram. However to find the background slope, the surface should only be fitted over the sound regions with the defective regions excluded from such calculation. To do so, the surface is first fitted using all the pixels
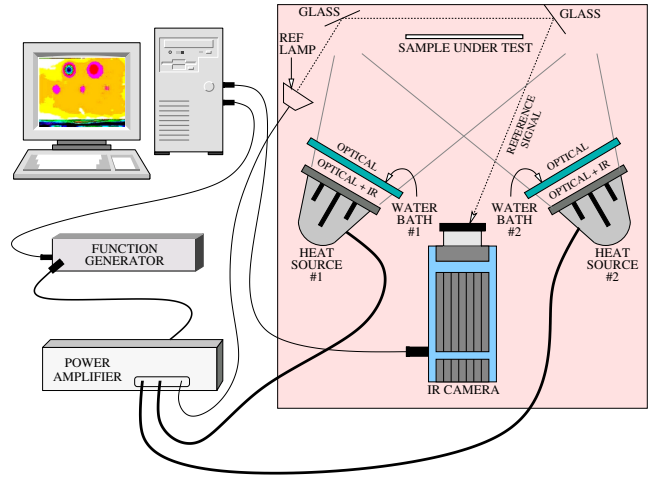

Figure 4: Experimental setup

of the thermogram and the standard deviation between the pixel data and the fitted surface is calculated. Then the surface is re-fitted excluding those pixels whose deviation lies outside the previously calculated standard deviation. The steps are repeated to exclude more and more defective area from the surface fit. From the practical point of view, three iterations were found sufficient for this purpose. The standard deviation between the pixel data and the fitted surface, which by now excludes the defective regions, is treated as noise.

6. Experimental setup

For all the pulsed, lock-in and FMTWI testing a TWI Thermoscope system[9] with an Indigo Merlin camera was used. The ThermoScope system is an integrated pulsed thermographic system employing a medium wavelength infrared camera and an integrated flash heating system outputting a heating pulse of approximately 2 kJ for 2 ms. The Indigo Merlin is an electrically cooled InSb focal plane array (FPA) camera with a 12-bit digital output and a resolution of 320×256 (width $\times$ height). The camera has a maximum frame-rate of 60 Hz and an NEdT of less than 25 mK (and typically < 18 mK).

For the pulsed testing, the camera was attached to a flash hood containing the high power flash lamp. For the lock-in and FMTWI tests, the camera was removed from the flash hood and 1000 Watt tungsten-halogen flood lamps were used to generate the sinusoidal and chirp heating of the sample surface, using a signal generator and amplifier to power the lamps. The surface temperatures in all cases were recorded using the same Indigo Merlin camera and ThermoScope system.

IR screens, consisting of glass tanks containing water (30 mm of water and 5 mm glass on each side), were used to remove the IR radiation emitted by the flood lamps that may have interfered with the lock-in and FMTWI tests. Also a smaller 500 Watt reference lamp was placed inside the setup which is seen through two glass reflectors to cut down its intensity. Testing was carried out to determine input voltages for the lamps
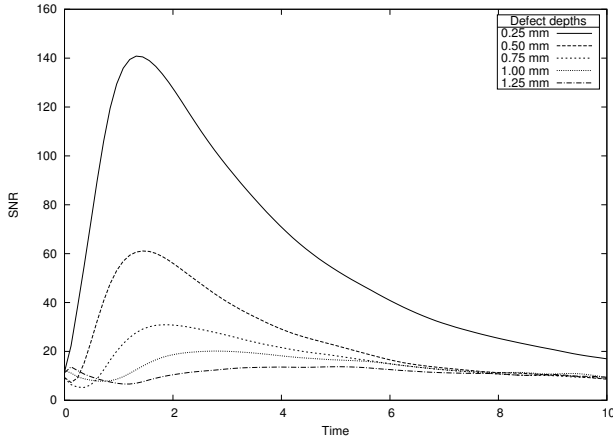
Figure 6: SNR as a function of time for 6 mm diameter defects at depths indicated in this figure.

Table 4: Maximum SNRs and their time of occurrence for 6 mm diameter defects in pulsed thermography experiment

Depth (mm)	Maximum SNR	Time of occurrence (second)
0.25	141	1.3
0.50	61	1.5
0.75	31	1.9
1.00	20	2.8
1.25	14	4.5

in order to obtain as pure a single-frequency sinusoid as possible to avoid wasting excitation energy and complicating the analysis of the results. Also -45° bulk phase lag with respect to the reference signal was verified to confirm that no direct IR reflection was coming from the sample[10].

7. Results

7.1. Pulsed thermography

The raw frames from the pulsed thermography experiment are shown in figure 5. It is found that the signal-to-noise ratio exhibits time variation as both the noise floor and the signal magnitude change with frames. The plots of the SNRs vs time for the 6 mm defects are shown in figure 6. It clearly shows that for each defect, there exists a frame where its signal-to-noise ratio becomes maximum. These best SNRs, which are listed in table 4, are chosen for comparison with the data obtained from lock-in and FMTWI.

7.2. Lock-in thermography

The magnitude and phase images obtained by lock-in thermography at 16.7 mHz, 33.3 mHz, 50.0 mHz, 66.7 mHz and 83.3 mHz using the algorithm describe in section 5.1 are shown in figure 7a to 7e and figure 8a to 8e respectively. Each of the lock-in runs consists of three complete excitation cycles as mentioned earlier in section 3. The images are displayed after their backgrounds are subtracted using surface fit as described in section 5.2.1. As predicted by the one dimensional heat propagation model, the magnitude images reveal deeper defects only at lower frequencies as the thermal waves penetrate deeper into the material. Also the magnitude increases with frequency, which is evident from the gray-scale bar shown inside the figure, as more energy is pumped-in at higher frequencies because of reduced test duration and the matched energy condition. It is note-worthy in the phase images that the phase value of the shallow defects change sign as the frequency is increased. The frequency at which the phase response crosses zero is called the blind frequency. The name is appropriate, as at this frequency, the defect merges with the sound background making it hard to detect. Figure 9a shows the plot of phase response obtained from lock-in tests as a function of excitation frequency. The zero-crossings are obvious.

The signal-to-noise ratio obtained from the lock-in magnitude and phase images at the aforesaid frequencies by using the algorithm describe in section 5.2, are tabulated in table 5 and are plotted in figure 9c and 9e respectively. The phase SNR goes through a minimum because of blind frequencies.

7.3. FMTWI

The FMTWI test was performed with a 20 mHz to 80 mHz, 60 seconds linear up-chirp. As discussed earlier in section 3, the chirp signal consisted of three complete oscillation having identical initial and final phase. The data processing is similar to that of the lock-in test. The magnitude and phase images generated at 16.7 mHz, 33.3 mHz, 50.0 mHz, 66.7 mHz and 83.3 mHz from the FMTWI test are shown in figure 7f to 7j and figure 8f to 8j respectively. Visibly, these images are similar to those of lock-in which are shown together for easy comparison. One major difference in the magnitude image is the gray-scale values which does not increase with frequency as it did in the case of lock-in. Rather as the chirp spans over the 20 mHz to 80 mHz frequency range, energy content at 16.7 mHz and 83.3 mHz falls significantly. However, it does not deteriorate the image quality as the noise, which is primarily due to composite structure[11], also goes down with it. Hence signal-to-noise ratio is preserved. As our eyes are more sensitive to signal-to-noise ratio rather than the absolute noise or signal, the deterioration does not affect the appearance of the gray-scale image.

The phase images demonstrated similar blind frequency and sign change phenomena as in lock-in. But the advantage of using FMTWI is that all the phase and magnitude images can be generated from a single run. So if a defect is missed at one frequency because of the blind frequency effect, it will be visible at other frequencies. The plots of phase vs. frequency obtained from the FMTWI test for 6 mm diameter defects are shown in figure 9b along with their lock-in counterpart. The plots of signal-to-noise ratio obtained from magnitude and phase images for the same 6 mm diameter

(a) t = 1.3 second   (b) t = 1.5 second   (c) t = 1.9 second   (d) t = 2.8 second   (e) t = 4.5 second
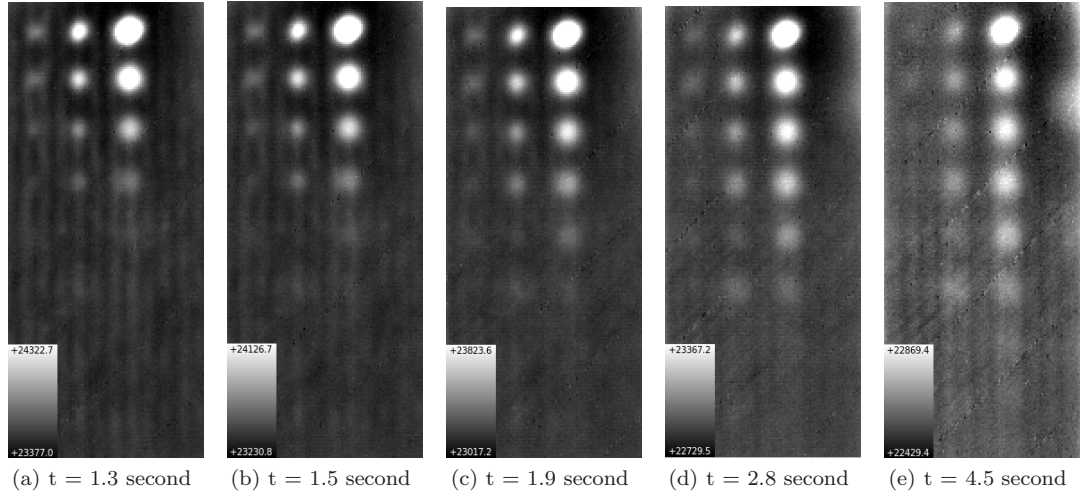
Figure 5: Pulsed thermography frames with maximum SNR for each of the 6 mm diameter defects mentioned in table 4. The scale bar indicates the range of digital levels covered by the thermal image.

(a) Lock-in magnitude image at 16.7 mHz

(b) Lock-in magnitude image at 33.3 mHz

(c) Lock-in magnitude image at 50.0 mHz

(d) Lock-in magnitude image at 66.7 mHz

(e) Lock-in magnitude image at 83.3 mHz

(f) FMTWI magnitude image at 16.7 mHz

(g) FMTWI magnitude image at 33.3 mHz

(h) FMTWI magnitude image at 50.0 mHz

(i) FMTWI magnitude image at 66.7 mHz
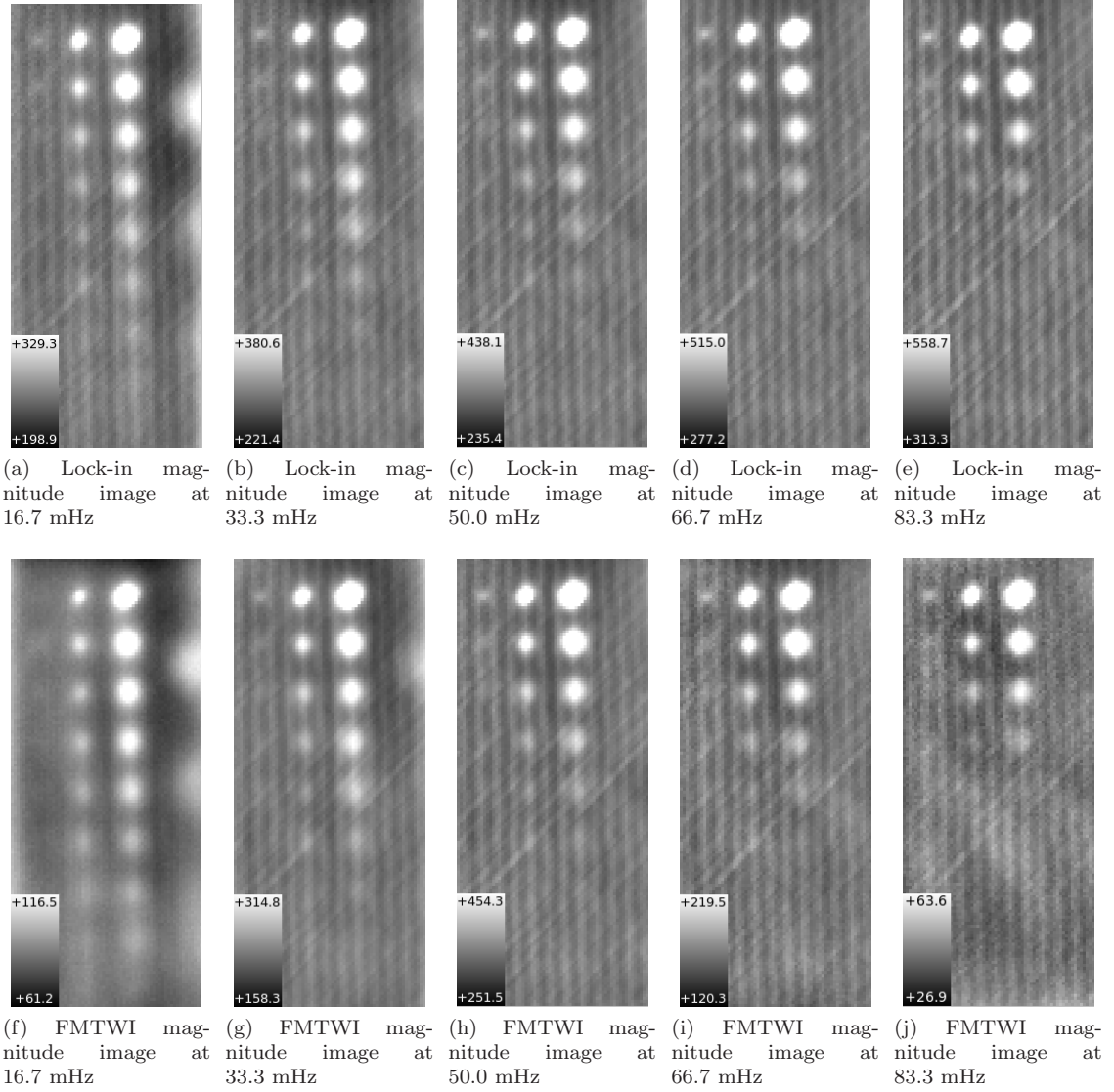
(j) FMTWI magnitude image at 83.3 mHz

Figure 7: Experimental magnitude images at 16.7 mHz, 33.3 mHz, 50.0 mHz, 66.7 mHz and 83.3 mHz for lock-in thermography (7a-7e), and FMTWI (7f-7j), respectively.
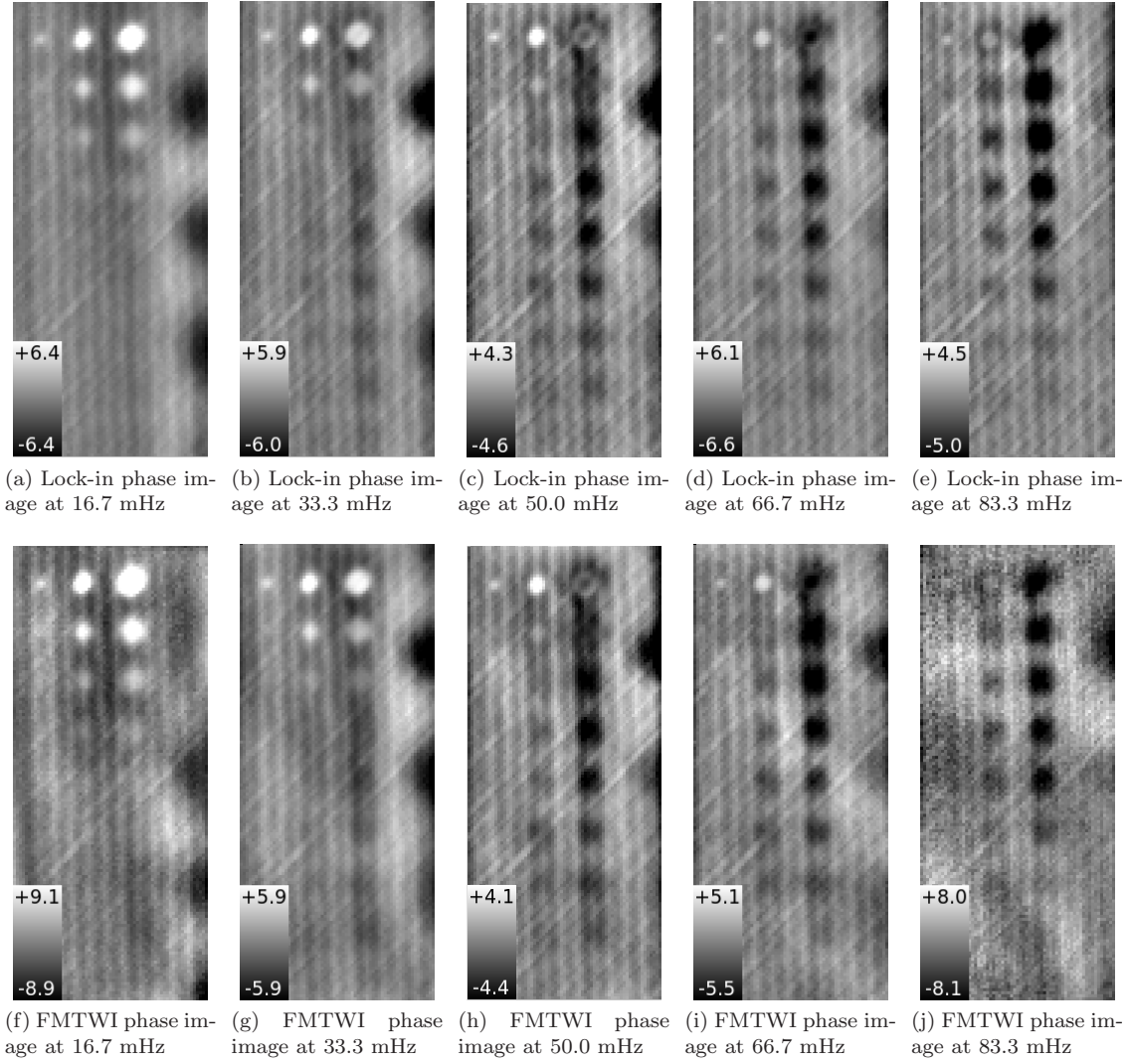
9

(a) Lock-in phase image at 16.7 mHz (b) Lock-in phase image at 33.3 mHz (c) Lock-in phase image at 50.0 mHz (d) Lock-in phase image at 66.7 mHz (e) Lock-in phase image at 83.3 mHz

(f) FMTWI phase image at 16.7 mHz (g) FMTWI phase image at 33.3 mHz (h) FMTWI phase image at 50.0 mHz (i) FMTWI phase image at 66.7 mHz (j) FMTWI phase image at 83.3 mHz

Figure 8: Experimental phase images at 16.7 mHz, 33.3 mHz, 50.0 mHz, 66.7 mHz and 83.3 mHz for lock-in thermography (8a-8e), and FMTWI (8f-8j), respectively.

defects are shown in figure 9d and 9f respectively. The marked similarity with the lock-in results is obvious.

7.4. Comparison of the best pulsed, lock-in and FMTWI images

A comparison of the best pulsed, lock-in and FMTWI images is summarized in figure 10 and table 6. It shows that for the shallowest defect, pulsed thermography produces the best signal-to-noise ratio, and lock-in and FMTWI magnitude images follow. It is interesting to note that the phase images produce the worst signal-to-noise ratio. For the deeper 1.25 mm defect, all techniques turn out to be equally good/bad.

8. Comparison with TSR

It may be considered unfair to compare the raw pulsed images with mathematically processed amplitude and phase images obtained from the lock-in and FMTWI experiments. Thus, to make a fair comparison, the pulsed images were enhanced with the time series reconstruction (TSR) algorithm[12]. Steps followed are summarized below:
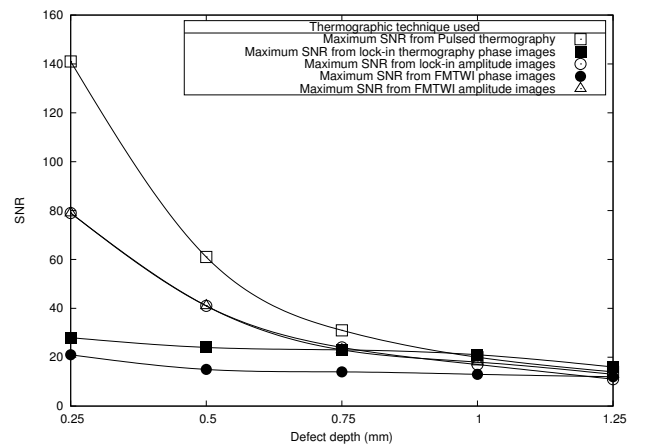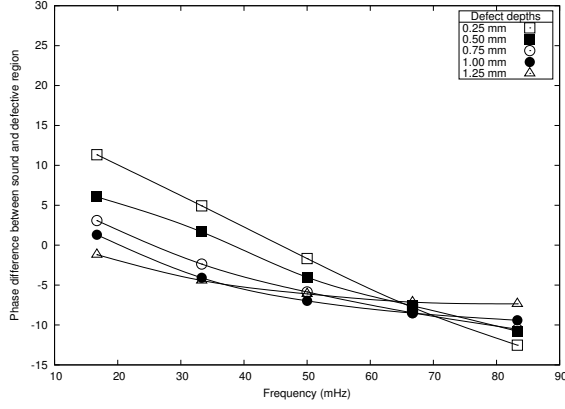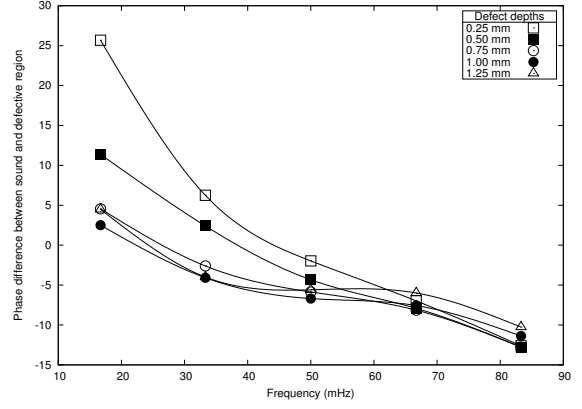

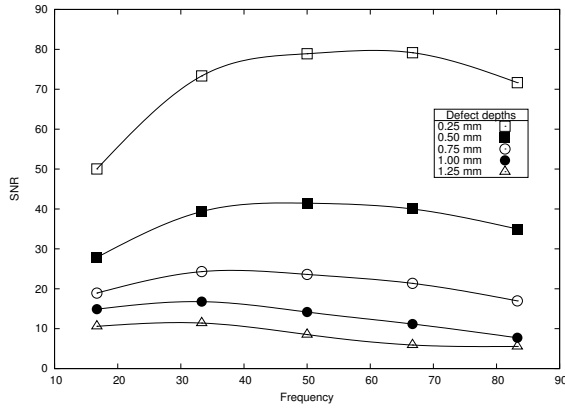Figure 10: Plot of maximum SNR as a function of defect depth, as in Table 6

- The average of pre-flash frames was subtracted from the rest of the pulsed experiment video.
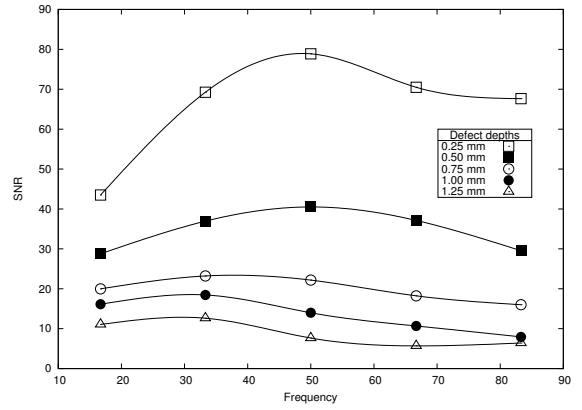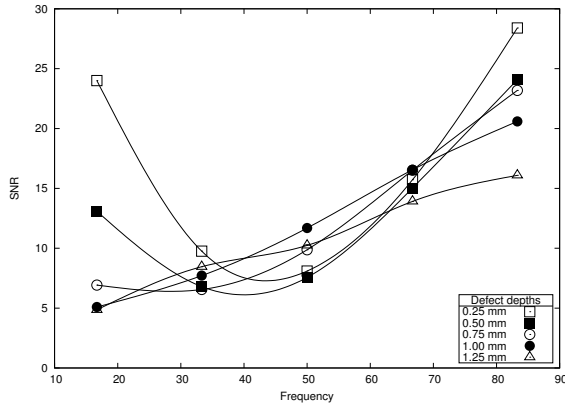
(a) Lock-in phase response vs Frequency

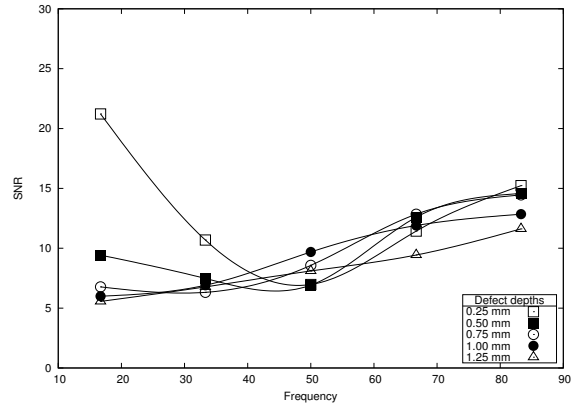(b) FMTWI phase response vs. Frequency

(c) Lock-in magnitude SNR vs Frequency

(d) FMTWI magnitude SNR vs. Frequency

(e) Lock-in phase SNR vs Frequency

(f) FMTWI phase SNR vs. Frequency

Figure 9: 9a & 9b: Phase difference between sound and defect regions analyzed as a function of frequency for lock-in and FMTWI tests for indicated defects. 9c & 9d: Plots of SNR observed in magnitude images of lock-in and FMTWI tests as a function of analysis frequency. 9e & 9f: Plots of SNR observed in phase images of lock-in and FMTWI tests as a function of analysis frequency.

- Polynomials of the form $y = a_0 + a_1x + a_2x^2 + a_3x^3 + a_4x^4$ were fitted to the logarithmic time vs logarithmic temperature change data pixel-by-pixel. *i.e.* $x \equiv \log(t - t_F)$ where t_F: the time of the flash frame and $y \equiv \log(T - T_F)$ where T_F: the average of pre-flash frames' temperature at the corresponding pixels.

- Having the coefficients (a_i's) been calculated, the time vs. temperature change data were mathe-

matically reconstructed pixel-by-pixel by evaluating the corresponding polynomials at the sampling intervals of the original pulsed video.

- Two more videos were generated by taking the first and the second derivatives of the fitted polynomials — *i.e.* $y' = a_1 + a_2x + a_3x^2 + a_4x^3$ and $y'' = a_2 + a_3x + a_4x^2$ — and once again evaluating them pixel-by-pixel at intervals used above.

11

Table 5: SNR at various analysis frequencies, of magnitude and phase images obtained from lock-in and FMTWI tests. The maximum value observed for each defect is boxed.

Technique	Freq. (mHz)	SNR from magnitude images Defect depths (mm)					SNR from Phase images Defect depths (mm)				
		0.25	0.50	0.75	1.00	1.25	0.25	0.50	0.75	1.00	1.25
lock-in	16.7	50	28	19	15	11	24	13	7	5	5
	33.3	73	39	[24]	[17]	[11]	10	7	7	8	9
	50.0	[79]	[41]	24	14	9	8	8	10	12	10
	66.7	79	40	21	11	6	16	15	17	17	14
	83.3	72	35	17	8	6	[28]	[24]	[23]	[21]	[16]
FMTWI	16.7	43	29	20	16	11	[21]	9	7	6	6
	33.3	69	37	[23]	[18]	[13]	11	7	6	7	7
	50.0	[79]	[41]	22	14	8	7	7	9	10	8
	66.7	70	37	18	11	6	11	13	13	12	9
	83.3	68	30	16	8	6	15	[15]	[14]	[13]	[12]

Table 6: Maximum SNR obtained for various 6 mm diameter defects at indicated depths, for pulsed, lock-in and FMTWI tests.

Defect depth mm	Pulsed thermography	Lock-in thermography		FMTWI	
		Phase image	magnitude Image	Phase image	magnitude image
0.25	141	28	79	21	79
0.50	61	24	41	15	41
0.75	31	23	24	14	23
1.00	20	21	17	13	18
1.25	14	16	11	12	13

(a) SNR from TSR
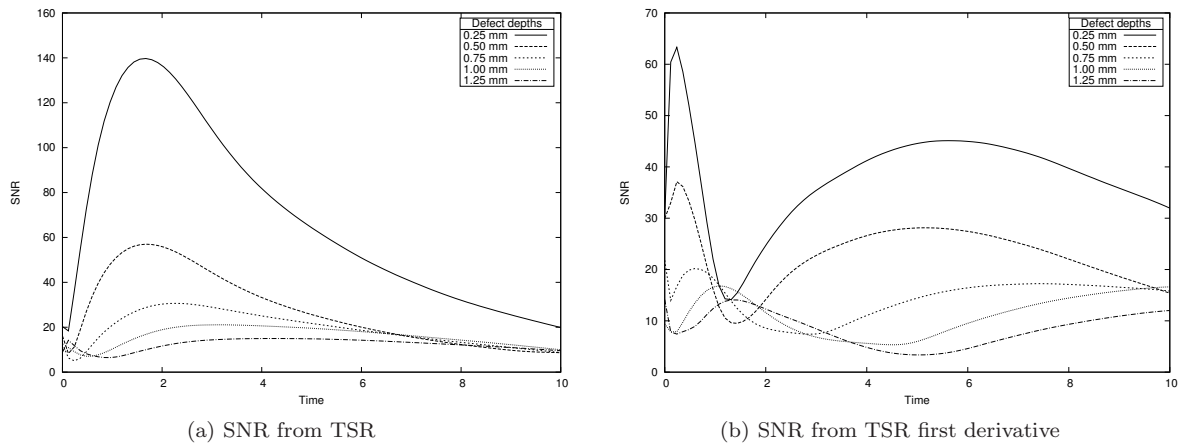

(b) SNR from TSR first derivative

Figure 11: SNR obtained from pulsed TSR and its derivatives.

The SNR algorithm, described in section 5.2, was run on the TSR and its derivative videos, and SNR plots were obtained (figure 11) for the five shallowest defects. It was found that the SNR obtained from the TSR video (figure 11a) was almost identical to that obtained from the raw pulsed video (figure 6). This is not surprising as the TSR is merely a polynomial fit of the raw data. However, it was unexpected that the TSR first deriva-

(a) Pulsed raw @ 6.3sec (b) Pulsed TSR @ 8.3sec (c) Pulsed TSR first derivative @ 4.7sec (d) Pulsed TSR second derivative @ 10sec (e) Amplitude image @ 16mHz (f) Phase image @ 50mHz
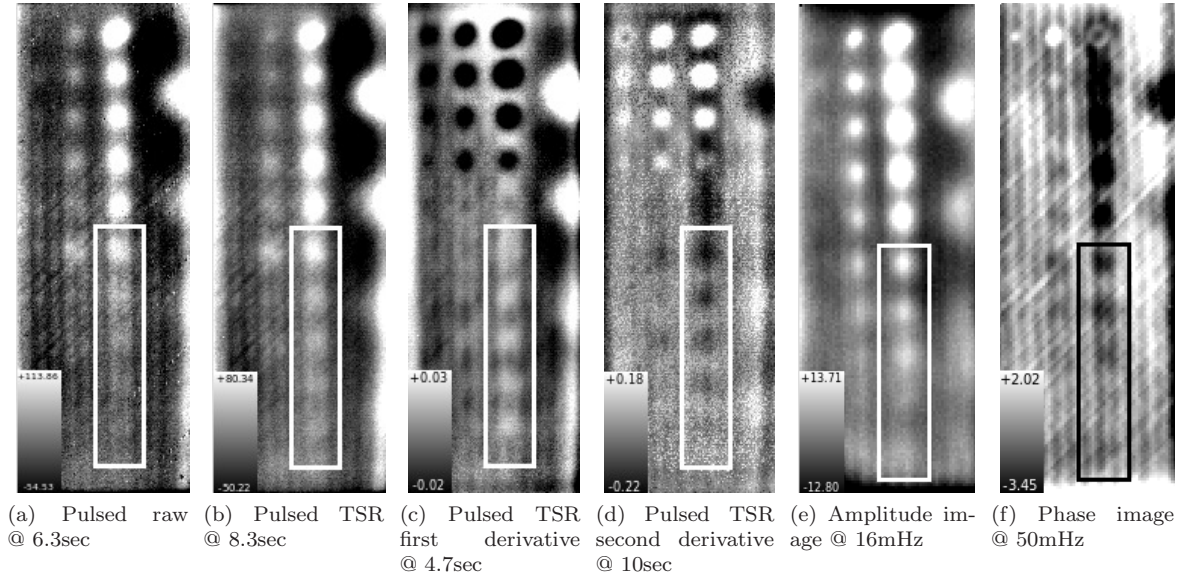
Figure 12: Comparison with TSR

tive produced a lower SNR (figure 11b).

The analysis was therefore extended further from five shallowest defects to the tenth defect in the row of 6mm diameter defects. The five, newly considered deeper defects span a depth of 1.5mm to 2.5mm in steps of 0.25mm. Even though, some of these deeper defects seemed to be visibly present, the SNR algorithm did not produce any meaningful result for them. The reason of its failure is that it cannot differentiate between structural patterns and those produced by the defects. So a qualitative comparison based on the visual appearance of the defects was carried out.

Figure 12 shows the best visual images obtained from the TSR and its derivatives along with the best looking amplitude and phase images obtained from FMTWI. Being identical to FMTWI, lock-in phase and amplitude images are omitted. The image contrast was adjusted on the basis of the region, marked with the rectangular box in the figure, where the deeper defects lie. While the raw pulsed image (figure 12a) could not reveal the deepest 6mm diameter defect being considered (*i.e.* 2.5mm deep), the TSR image (figure 12b) did show a blur. The best image of this defect was produced by the TSR first derivative image (figure 12c). Although the SNR value went down for the five shallower defects in TSR first derivative images (figure 11b), it revealed the deeper ones. This reduction in SNR of the shallower defects does not decline the performance of the TSR algorithm as a whole. This is because of the contrast adjustment carried out over the selected defect regions (outlined rectangles), which saturates the shallower defect to either pure white or black in the visual image irrespective of their SNR. It may be noted that the 16mHz FMTWI amplitude image also revealed most of the deeper defects.

9. FMTWI image fusion

The presence of blind frequencies imposes a risk of overlooking defects by the lock-in technique, if the frequency is not chosen correctly. Thus in lock-in tests, a set of frequencies have to be tried out to confirm that no such anomalies have occurred. This obviously would increase the duration of the test. However in FMTWI, it is possible to extract all the phase images from a single run. Hence it is considerably faster.

In principle, in FMTWI, it should be possible to obtain a fused image from the superposition of images at various component frequencies, such that the effect of blind frequencies is eliminated. One such algorithm is suggested for this purpose.

9.1. Algorithm

1. The phase images are extracted at specific frequencies which completes integral number of oscillations within the duration of the run and approximately falls within the bandwidth of the chirp. For a 60 seconds chirp with frequency sweep from 20 mHz to 80 mHz, these frequencies are 16.7 mHz, 33.3 mHz, 50.0 mHz, 66.7 mHz and 83.3 mHz.

2. The background value of each of the images are calculated and subsequently subtracted such that the pixel values gets equally distributed around zero. The surface fit described in section 5.2.1 is used to achieve this.

3. The images are normalized with one standard deviation mapped to unity.

4. All the pixel values are replaced with their absolute values.

5. The resulting background subtracted normalized absolute images are added together to manifest all the defects in a single image.

The algorithm was applied on the phase images generated from the FMTWI test and the final fused image is

13

Figure 13: Fused image obtained from the extracted FMTWI phase images at the five analysis frequencies.

shown in Figure 13. This image overcome all the blind frequency anomalies evident in the individual modulation frequency phase images shown in figure 8 whilst retaining the recognized advantages of phase imaging.

10. Conclusion

In this paper, three thermographic techniques (*viz* pulsed, lock-in and FMTWI) are compared based on effective excitation energy matching in time domain. It is shown that while for shallow defects in CFRP sample, the pulsed technique provides the best signal-to-noise ratio, its performance decreases for deeper defects. However, first derivative images obtained from TSR processed pulsed data show significant improvement in the detectability of the deeper features. Also, for these defects, lock-in and FMTWI become comparable to, if not better than the raw pulsed technique. FMTWI then has an edge over lock-in, in that the effect of overlooking some defects due to the blind frequency effect, is overcome. It has been found that the noise in the thermal images is dominated by the structural inhomogeneity of CFRP. This spatial domain noise is not reduced significantly by the techniques investigated here which only deal effectively with conventional time domain system noise. It would be interesting to repeat a similar comparison of the performance of the techniques at dealing with defects in a homogeneous material, such as mild steel, where structural noise should be absent. It would also be valuable to include in the comparison

pulse phase thermography which provides a means of obtaining phase images of defects from pulsed thermography image data [13, 14]. Use of pulse compression on FMTWI data is also expected to improve the image quality in the case of steel, because the time-bandwidth product should be considerably larger than is practical for CFRP.

References

[1] J. M. Milne, W. N. Reynolds, The non-destructive evaluation of composites and other materials by thermal pulse video thermography, Proceeding SPIE (1985) 119–22.

[2] S. K. Lau, D. P. Almond, J. M. Milne, A quantitative analysis of pulsed video thermography, NDT&E International 24 (1991) 195–202.

[3] G. Busse, D. Wu, W. Karpen, Thermal wave imaging with phase sensitive modulated thermography, Journal of Applied Physics 71 (1992) 3962.

[4] S. G. Pickering, D. P. Almond, Matched excitation energy comparison of the pulse and lock-in thermography nde techniques, NDT&E International 41 (2008) 501–509.

[5] W. Bai, B. S. Wong, Evaluation of defects in composite plates under convective environments using lock-in thermography, Measurement Science and Technology 12 (2001) 142–150.

[6] C. Wallbrink, S. A. Wade, R. Jones, The effect of size on the quantitative estimation of defect depth in steel structures using lock-in thermography, Journal of Applied Physics 101 (2007) 104907–8.

[7] S. Tuli, R. Mulaveesala, Defect detection by pulse compression in frequency modulated thermal wave imaging, Quantitative Infrared Thermography (QIRT) 2 (1) (2005) 41.

[8] S. Tuli, R. Mulaveesala, Theory of frequency modulated thermal wave imaging for nondestructive subsurface defect detection, Applied Physics Letters 89 (doi: 10.1063/1.2382738) (2006) 191913.

[9] Thermal Wave Imaging Inc. http://www.thermalwave.com/.

[10] D. P. Almond, P. M. Patel, Photothermal science and techniques, Chapman-Hall, 1996.

[11] S. G. Pickering, D. P. Almond, An evaluation of the performance of an uncooled microbolometer array infrared camera for transient thermography nde, Nondestructive Testing and Evaluation 22 (2007) 63–70.

[12] S. M. Shepard, J. R. Lhota, B. A. Rubadeux, D. Wang, T. Ahmed, Reconstruction and enhancement of active thermographic image sequences, SPIE Optical Engineering 42 (5) (2003) 1337–1342.

[13] X. V. Maldague, S. Marinetti, Pulse phase infrared thermography, Journal of Applied Physics 79 (5) (March 1996) 2694–2698.

[14] X. V. Maldague, F. Galmiche, A. Ziadi, Advances in pulsed phase thermography, Elsevier Infrared Physics & Technology 43 (2002) 175–181.